

Region-Specific Coarse Quantization with Check Node Awareness in 5G-LDPC Decoding

Philipp Mohr[✉], *Student Member, IEEE*, and Gerhard Bauch, *Fellow, IEEE*

Abstract—This paper presents novel techniques for improving the error correction performance and reducing the complexity of coarsely quantized 5G-LDPC decoders. The proposed decoder design supports arbitrary message-passing schedules on a base-matrix level by modeling exchanged messages with entry-specific discrete random variables. Variable nodes (VNs) and check nodes (CNs) involve compression operations designed using the information bottleneck method to maximize preserved mutual information between code bits and quantized messages. We introduce alignment regions that assign the messages to groups with aligned reliability levels to decrease the number of individual design parameters. Group compositions with degree-specific separation of messages improve performance by up to 0.4 dB. Further, we generalize our recently proposed CN-aware quantizer design to irregular LDPC codes and layered schedules. The method optimizes the VN quantizer to maximize preserved mutual information at the output of the subsequent CN update, enhancing performance by up to 0.2 dB. A schedule optimization modifies the order of layer updates, reducing the average iteration count by up to 35 %. We integrate all new techniques in a rate-compatible decoder design by extending the alignment regions along a rate-dimension. Our complexity analysis for 2-bit decoding estimates up to 64 % higher throughput versus 4-bit decoding at similar performance.

Index Terms—LDPC decoder, layered decoding, rate-compatible, coarse quantization, information bottleneck

I. INTRODUCTION

SINCE their invention by Gallager [1] and rediscovery by MacKay [2], low-density parity-check (LDPC) codes have become a crucial component in the field of modern communication systems. One important application is 5G [3], where LDPC codes can achieve near-capacity performance with highly parallel belief propagation decoding [1], [2].

However, a significant bottleneck in belief propagation is the massive exchange of messages between variable nodes (VNs) and check nodes (CNs). Therefore, many works focused on reducing the bit width of the exchanged messages through quantization [4]–[21]. Conventional approaches approximate the belief propagation algorithms with sub-optimal quantization operations aiming at low-complexity implementations [5]. Another direction is to design operations that maximize preservation of mutual information within the exchanged messages [6]–[21]. These decoders can achieve excellent performance at lower message resolutions than the conventional techniques.

Quantized belief propagation was discovered by Thorpe *et al.* [6], [7] where node operations aim at maximizing preserved mutual information between code bits and exchanged

messages. The node operations exploit a computational domain that merges multiple inputs into a compressed output message via arithmetic operations and a final quantization step. The idea of using mutual information maximizing quantization in the decoder was pushed further by Kurkoski *et al.* [8] where all internal node operations perform compression mappings realized with two-input lookup tables (LUTs).

For the computational and the LUT decoder the fundamental challenge is to design compression mappings that assign observed messages to a compressed message under preservation of relevant information. The information bottleneck (IB) method describes this problem with a relevant, observed, and compressed variable and can design compression mappings that maximize the mutual information between the compressed and relevant variable [9], [11], [22].

Another challenge arises when a decoder stage includes nodes with different degrees, resulting in messages with different alphabets of reliability levels. Addressing these alphabets across subsequent decoder stages can lead to an unmanageable variety of LUTs. *Message alignment* was proposed in [23] which can be used to design decoder stages so that output messages refer to the same reliability alphabet. The technique enabled rate-compatible LUT decoders for 5G codes in [13] with aligned messages between consecutive decoder stages.

He *et al.* [14] combined the original quantized belief propagation approach of [7] with the information-optimum algorithm of [9]. The combination resulted in better performance than the two-input LUT decoders which suffer from consecutive compression steps within each node update.

Another highly relevant aspect is the composition and order of decoder stages determined by the decoding schedule. A layered schedule subdivides the parity check matrix into layers and can halve the required number of message updates compared to a flooding schedule [24]. Our works [15], [18] extended the mutual information maximizing decoding algorithms to row- and column-layered decoding for regular LDPC codes with computational domain and LUT decoders. Kang *et al.* [20] developed a computational domain decoder design that supports column-layered decoding of irregular LDPC codes. Lv *et al.* [25] proposed an entry-specific decoder design but investigated only a high-rate code.

This work develops mutual information maximizing techniques focusing on 5G LDPC codes [3]. The wide range of node degrees and required support for rate compatibility make the decoder design for very coarse quantization challenging. We propose several techniques to improve the current state-of-the-art with the following contributions:

- Section III introduces a probabilistic memory model

Philipp Mohr and Gerhard Bauch are with the Institute of Communications, Hamburg University of Technology, Hamburg, 21073, Germany. E-mail: {philipp.mohr; bauch}@tuhh.de.

that characterizes the exchanged messages on a base-matrix level. The derived mutual information maximizing decoders are compatible with *arbitrary schedules* that operate on the memory model. The focus lies on compatibility with the 5G LDPC codes by accurately tracking the effect of punctured and filler bits on a base-matrix level. A dedicated initialization procedure is used, proposed in section II, to avoid useless updates resulting from processing punctured inputs.

- The concept of alignment regions is developed in section IV that defines subsets of exchanged messages. All messages in the subset can be associated with reliability levels from a common alphabet for reducing the variety of decoder parameters. We show that the size and organization of subsets significantly influence the decoding performance.
- Section V develops a CN aware quantizer design at the VN assuming a min-sum operation at the CN. The contribution extends our work [17] to irregular LDPC codes and layered schedules. A reformulation allows the optimization of non-uniform quantization thresholds using the IB method. The extended design can enhance the performance beyond the mutual information maximizing decoding of [14], particularly for 2-bit decoding.
- In section VII, an optimization of the row- and column-layered schedules is proposed. The resulting schedule defines an optimized order of layers that maximizes the mutual information under coarse quantization after every update step.
- We develop a rate-compatible design in section VIII that reuses the approach in section IV by extending the alignment regions with a rate-dimension.
- Different implementation structures are compared in section IX. The 2-bit decoding leads to very efficient structures, offering an estimated 64% higher throughput versus 4-bit decoding at the same frame error rate performance.

II. ENCODING AND DECODING OF 5G LDPC CODES

This section describes matrix and graph representations of 5G-LDPC codes. We use these representations to define LDPC decoding with arbitrary message passing schedules, such as a flooding or layered schedule. Further, an efficient initialization schedule is introduced to avoid useless decoder operations due to punctured code bits.

A. Preliminaries

Most standards define LDPC codes through a base matrix $\mathbf{H}_b \in \{-1, \dots, Z\}^{N_b^c \times N_b^v}$ highlighted with a blue rectangle in Fig. 1a for a 5G-LDPC code. A lifting procedure replaces every entry H_b^{ij} of \mathbf{H}_b with a $Z \times Z$ square matrix to obtain the full parity check matrix \mathbf{H} as shown in Fig. 1b. The non-negative entries H_b^{ij} (gray, Fig. 1a) turn into cyclic H_b^{ij} -right-shifted identity matrices. The other entries (white) turn into zero matrices. The encoder maps the information bits $\mathbf{u} \in \{0, 1\}^K$ to code bits $\mathbf{b} \in \{0, 1\}^M$ such that $\mathbf{H}\mathbf{b} = \mathbf{0}$.

In 5G NR the base matrix \mathbf{H}_b is obtained from one of the two template base matrices (termed base graph 1 and 2)

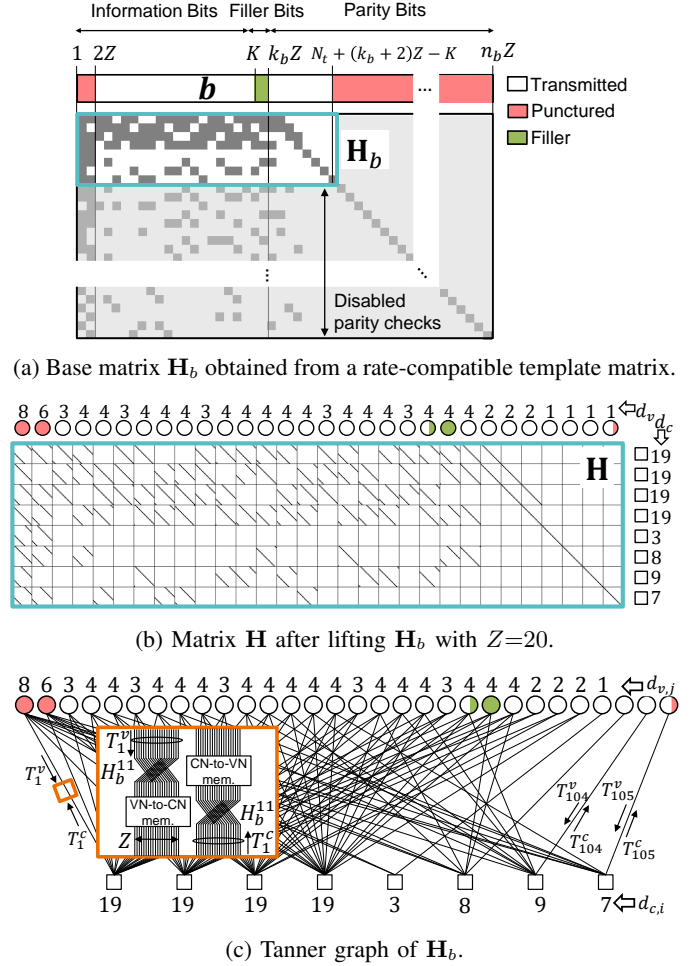


Fig. 1: Representations of 5G-LDPC codes.

depending on the desired code rate r as well as the desired information block lengths K [3]. Base graph 2 is used if $K \leq 292$, $r \leq 0.25$, or $r \leq 0.67$ and $K \leq 3824$. Otherwise base graph 1 is selected. Fig. 1a depicts base graph 1 designed for rates $r = \frac{1}{3}$ to $\frac{22}{24}$ [26]. The maximum lifting size is chosen from a table satisfying $K \leq k_b Z$ where $k_b = 22$. As indicated in Fig. 1a, the information bits \mathbf{u} are placed at positions 1 to K . Fine granularity for choosing K is enabled when allowing filler bits at positions $K+1$ to $k_b Z$ known by the receiver.

The parity bits are computed using the information and filler bits [27]. From the full code word only $N_t = \lceil K/r \rceil$ bits are selected for transmission as shown in Fig. 1a. Parity checks that involve two punctured bits are disabled, decreasing the size of the base matrix \mathbf{H}_b to $N_b^c = 2 + \lceil \frac{N_t - K}{Z} \rceil$ rows and $N_b^v = k_b + N_b^c$ columns.

The decoder observes channel log-likelihood ratios (LLRs) $L_m^{ch} = \log \frac{p(b_m=0|\mathbf{y}^{ch})}{p(b_m=1|\mathbf{y}^{ch})}$ for a received channel sequence \mathbf{y}^{ch} . The LLRs L_m^{ch} are 0 for the punctured positions and ∞ for the filler positions.

B. Message Passing Decoding with Arbitrary Schedules

The base matrix \mathbf{H}_b can be represented by a Tanner graph illustrated in Fig. 1c. Each column j turns into a variable node (VN) and each row i into a check node (CN). The edges between VNs and CNs represent non-negative entries H_b^{ij} . The

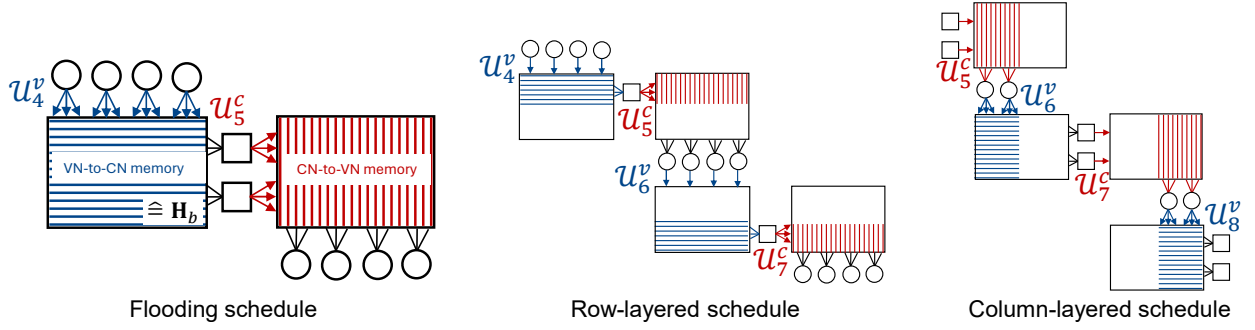


Fig. 2: Illustrations of different schedules for one iteration after initialization with unrolled VN and CN memory updates.

node degree, i.e., the number of connected edges to a node, is $d_{v,j}$ for a VN and $d_{c,i}$ for a CN.

Message passing decoding computes and exchanges messages between VNs and CNs to aggregate soft information for error correction from the parity check constraints. Each edge of the graph contains a VN and CN memory location enumerated with $n \in \mathcal{N} = \{1, \dots, \sum_j d_{v,j}\}$ for VN-to-CN and CN-to-VN messages, respectively. A memory location stores Z messages after lifting the graph as illustrated within the orange box in Fig. 1c. The sets $\mathcal{U}^v \subseteq \mathcal{N}$ and $\mathcal{U}^c \subseteq \mathcal{N}$ specify target memory locations for VN and CN updates, respectively. The decoding schedule defines the order in which memory locations are updated as

$$\mathcal{U} = (\mathcal{U}_0^v, \mathcal{U}_1^c, \mathcal{U}_2^v, \mathcal{U}_3^c, \dots) \quad (1)$$

followed by a final hard decision update that uses the most recent updated CN messages.

Fig. 2 illustrates three schedule types for one decoder iteration after initialization (see section II-C). One iteration involves updating a total of $2|\mathcal{N}|$ memory locations through multiple node updates.

A flooding schedule updates all VN memory locations \mathcal{U}_4^v followed by updating all CN memory locations \mathcal{U}_5^c .

In a row-layered schedule the parity check matrix is divided into multiple sets of rows called *layers*. In Fig. 2 the memory locations corresponding to the first layer \mathcal{U}_4^v and \mathcal{U}_5^c are updated with VNs and CNs, respectively. Hence, the second layer observes improved reliability information from the first layer for updating \mathcal{U}_6^v and \mathcal{U}_7^c . One iteration results in better error correction performance compared to a flooding schedule.

In a column-layered schedule, the parity check matrix is divided into multiple sets of columns. In Fig. 2 the memory locations corresponding to the first layer \mathcal{U}_5^c and \mathcal{U}_6^v are updated with CNs and VNs, respectively.

C. Initialization under 5G LDPC Codes

In the case of 5G LDPC codes the channel messages related to the first two columns are zero-LLRs due to puncturing (cf. Fig. 1). Hence, updating the corresponding VNs would create zero-LLR CN inputs. A CN update with at least a single extrinsic zero-LLR input leads to a zero-LLR output that is useless in further processing [28]. We carry out a fixed initialization sequence that omits CN updates connected to punctured VNs, avoiding useless updates. A simple but effective initialization is proposed as follows (cf. Fig. 1b):

- 1) \mathcal{U}_0^v and \mathcal{U}_1^c generate useful messages for memory-locations within the first column.
- 2) \mathcal{U}_2^v and \mathcal{U}_3^c generate useful messages for memory locations within the second column.
- 3) For the column-layered schedule, on top of the above steps, \mathcal{U}_4^v updates the remaining non-initialized VN-to-CN memory locations.

The initialization procedure saves complexity of about 1.5 decoding iterations compared to a standard schedule processing.

III. MUTUAL INFORMATION MAXIMIZING QUANTIZED DECODER DESIGN WITH ARBITRARY SCHEDULES

Limiting the bit width of the exchanged messages is crucial for reducing the storage and routing complexity in iterative message passing decoding. Hence, this section extends the decoder memory model from section II-B with mutual information maximizing compression operations. As a novelty, our formulation supports any decoding schedule leading to a location-specific design of operations with the application of the IB method [11]. Thus, every update of a VN and CN memory location is designed individually in sections III-B and III-C by accurately taking into account *location-dependent* distributions of messages resulting from the schedule, node degrees, punctured bits, and filler bits.

A channel quantizer for the channel LLRs L_m^{ch} is designed in section III-A whose outputs are modeled with the discrete random variables T_j^{ch} for every base-matrix column j . We model the encoded bits b_m with column-specific bit variables X_j^{ch} . A channel message variable T_j^{ch} shares a relationship to the relevant bit variable X_j^{ch} conveyed with the joint probability distribution $p(x_j^{ch}, t_j^{ch})$. Similarly, the exchanged messages between VNs and CNs in Fig. 1c are modeled using discrete random variables T_n^v and T_n^c for every memory location n . Each memory location can be associated with a relevant bit variable $X_n = X_{\text{col}(n)}^{ch}$. The distribution of exchanged messages w.r.t. relevant bits is tracked with discrete density evolution [4]. Table I summarizes all used random variables.

A. Mutual Information Maximizing Channel Quantization

For each encoded bit b_m , the channel quantizer observes a real-valued LLR L_m^{ch} that shall be quantized to a w^{ch} -bit message t_m^{ch} with minimal performance loss. The messages b_m, L_m^{ch} and t_m^{ch} can be modeled by three discrete random variables X, Y and T that form a Markov chain $X \rightarrow Y \rightarrow T$.

TABLE I: Random variables in the probabilistic model.

	Type	Channel	VN-to-CN	CN-to-VN
Relevant bit	variable	X_j^{ch}	$X_n = X_{\text{col}(n)}^{ch}$	X_n
	alphabet	$\mathcal{X}^{ch} = \{0, 1\}$	$\mathcal{X}_n = \mathcal{X}^{ch}$	\mathcal{X}_n
	realization	x_j^{ch}	$x_n = x_{\text{col}(n)}^{ch}$	x_n
Message	variable	T_j^{ch}	T_n^v	T_n^c
	bit width	w^{ch}	w^v	w^c
	alphabet	\mathcal{T}_j^{ch}	\mathcal{T}_n^v	\mathcal{T}_n^c
	realization	t_j^{ch}	t_n^v	t_n^c
$\mathcal{T}_\diamond = \{-2^{w^\diamond-1}, \dots, -1, 1, \dots, 2^{w^\diamond-1}\} \times \{\diamond\}$, $\diamond \in \{ch, v, c\}$, $\diamond \in \{j, n\}$ with base-matrix column j and memory location n .				

This kind of setup is covered by the IB framework where $X, x \in \mathcal{X}$ is the relevant variable, $Y, y \in \mathcal{Y}$ is the observed variable, and $T, t \in \mathcal{T}$ is the compressed variable [11]. The real-valued L^{ch} can be accurately modeled with a discrete variable Y through fine uniform quantization. From an information theoretic perspective, the mutual information $I(X; Y)$ upper bounds the achievable information rate. Thus, designing a compression mapping $p(t|y)$ with minimal mutual information loss $I(X; Y) - I(X; T)$ is considered as the information-optimum objective, i.e., $\max_{p(t|y)} I(X; T)$.

In [29] it was shown that for a binary alphabet \mathcal{X} that the optimal deterministic mapping $p(t|y)$ can be defined using a set of quantization thresholds $\tau = (\tau_0, \dots, \tau_{2^w})$ according to

$$t = Q(L(x|y)) = \mathcal{T}[k] \quad \tau_k \leq L(x|y) < \tau_{k+1}, 0 < k < |\tau| \quad (2)$$

with LLR $L(x|y) = \log(p(x=0|y)/p(x=1|y))$, outer thresholds $\tau_0 = -\infty$ and $\tau_{|\tau|-1} = +\infty$, and $\mathcal{T}[k]$ identifying the k th element of the ordered set \mathcal{T} .

Only the joint distribution $p(x, y)$ and the output message size $|\mathcal{T}|$ need to be specified before the optimization is performed. As in [16], symmetric thresholds are enforced with $\tau_k = -\tau_{|\tau|-k}$ and $\tau_{|\tau|/2} = 0$.

B. Quantized Variable Node Design with Arbitrary Schedules

In our probabilistic decoder model, VNs update the joint probability distributions $p(x_n, t_n^v)$ for all memory locations $n \in \mathcal{U}^v$ defined in a single step of the decoding schedule \mathcal{U} . This section designs a specific VN update for each memory location $n \in \mathcal{U}^v$ to maximize mutual information $I(X_n; T_n^v)$. A VN update for a memory location n in column $j = \text{col}(n)$ with degree $d = d_j^v$ combines a channel message t_j^{ch} and $d-1$ extrinsic CN messages $t_{n_k}^c$ into a compressed output message t_n^v . The indexing of output location n gives the extrinsic input locations $n_k = (n' : n' \neq n, \text{col}(n') = \text{col}(n))_k$. Any observed input combination

$$y_n^v = (t_j^{ch}, t_{n_1}^c, \dots, t_{n_d}^c) \in \mathcal{Y}_n^v = \mathcal{T}_j^{ch} \times \mathcal{T}_{n_1}^c \times \dots \times \mathcal{T}_{n_d}^c \quad (3)$$

provides extrinsic information about X_n . Fig. 3b shows a VN IB setup, where X_n, Y_n^v and T_n^v are the relevant, observed, and compressed variables X, Y and T , respectively. As in section III-A, an IB algorithm finds a mutual information maximizing compression mapping $p(t|y)$ realized with threshold quantization $t = Q(L(x|y))$ where [7]

$$L(x|y) = L(x) + \sum_{t' \in \mathcal{Y}} L(t'|x). \quad (4)$$

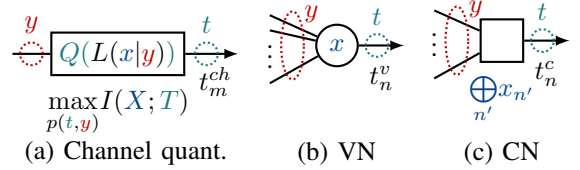


Fig. 3: IB setups for channel quantizer, VN and CN.

We remark that (4) assumes $p(t'|x, y \setminus \{t'\}) = p(t'|x) \forall t' \in \mathcal{Y}$ which neglects cycles of the lifted graph. The hard decision for the code bit x_n yields

$$\hat{x}_n = \begin{cases} 0 & \text{if } L(x_n | \hat{y}_n) > 0 \\ 1 & \text{otherwise} \end{cases} \quad (5)$$

where $\hat{y}_n \in \mathcal{Y}_n^v \times \mathcal{T}_n^c$ includes the non-extrinsic message.

In an implementation, (4) is considered as the computational part where the LLRs $L(t'|x)$ are reconstructed using lookup tables. The implementation and design complexity can be significantly reduced by processing w' -bit integer representations of the real-valued LLRs. The integer representations are obtained by scaling and rounding the underlying real numbers. Simulation results have shown that an LLR resolution of 0.05 is sufficient in the considered cases to avoid performance loss.

C. Quantized Check Node Design with Arbitrary Schedules

In our probabilistic decoder model, CNs update the joint probability distributions $p(x_n, t_n^c)$ for all memory locations $n \in \mathcal{U}^c$ defined in a single step of the decoding schedule \mathcal{U} . This section designs a specific CN update for each memory location $n \in \mathcal{U}^c$ to maximize mutual information $I(X_n; T_n^c)$. A CN update for a memory location n in row $i = \text{row}(n)$ with degree $d = d_i^c$ combines $d-1$ extrinsic VN messages $t_{n_k}^v$ into a compressed output message t_n^c . The indexing of output location n gives the extrinsic input locations $n_k = (n' : n' \neq n, \text{row}(n') = \text{row}(n))_k$. Any observed input combination

$$y_n^c = (t_{n_1}^v, \dots, t_{n_d}^v) \in \mathcal{Y}_n^c = \mathcal{T}_{n_1}^v \times \dots \times \mathcal{T}_{n_d}^v \quad (6)$$

provides extrinsic information about the variable X_n whose realization is constrained as $x_n = x_{n_1}^v \oplus \dots \oplus x_{n_d}^v$. Fig. 3c shows a CN IB setup, where X_n, Y_n^c and T_n^c are the relevant, observed and compressed variables X, Y and T , respectively. As in section III-A, an IB algorithm finds a mutual information maximizing compression mapping $p(t|y)$ realized with threshold quantization $t = Q(L(x|y))$ where [7]

$$L(x|y) = \prod_{t' \in \mathcal{Y}} \text{sgn}(L_{t'}) \cdot \phi^{-1} \left(\sum_{t' \in \mathcal{Y}} \phi(|L_{t'}|) \right) \quad (7)$$

with the reconstructed inputs obtained through

$$L_{t_l}^v = L(x_l^v | t_l^v) \text{ and } \phi(|L|) = -\log \tanh(|L|/2). \quad (8)$$

In an implementation, (7) is the computational part where the reconstruction uses a lookup table. The inverse transformation $\phi^{-1}(|L|) = \phi(|L|)$ is a monotonic decreasing w.r.t. $|L|$. Hence, computing ϕ^{-1} is not required as the threshold levels of Q can be shifted to include the inverse transformation.

With the min-sum approximation, (7) simplifies to

$$L(x|y) \approx \prod_{t' \in \mathcal{Y}} \text{sgn}(L_{t'}) \min_{t' \in \mathcal{Y}} (|L_{t'}|). \quad (9)$$

If all $t \in y$ use a sign-magnitude format and have equal LLR levels, the reconstruction and quantization operation can be removed without affecting the behavior [12], [30]:

$$t \approx \prod_{t' \in y} \text{sgn}(t') \min_{t' \in y}(|t'|) \quad (10)$$

IV. NODE DESIGN WITH ALIGNMENT REGIONS

In section III we designed individual quantizers for each message variable T_n^* where $\star=v$ labels a VN message and $\star=c$ labels a CN message. The message variables T_n^* model the exchanged decoder messages on a base-matrix level. Fig. 4a highlights the message variables T_n^* with *different* grayscale tones to indicate potentially different reliability levels associated with the memory locations n . The reliability levels $p(x_n|t_n^*)$ of a message t_n^* change with every node update and are mainly influenced by the node degrees and the decoding schedule.

In this section, an averaging operation is applied to the message variables T_n^* *before* the node design to reduce the variety of decoder parameters for reconstruction and quantization. Thus, average variables \bar{T}_a^* replace T_n^* in the *reconstructions* (4) with $\star=c$ and (7) with $\star=v$. The index $a \in \{1, \dots, |\mathcal{A}|\}$ identifies parts of the memory $\mathcal{N}_a \subseteq \mathcal{N}$ where \mathcal{N} is the set of all memory locations. Several examples for different averaging strategies are provided in Fig. 4b to 4e where the same grayscale tone indicates membership to the same averaging region \mathcal{N}_a . The average bit variables \bar{X}_a and average message variables \bar{T}_a^* are jointly distributed according to

$$p(\bar{X}_a=x, \bar{T}_a^*=t) = \sum_n p(n|a)p(X_n=x, T_n^*=t) \quad (11)$$

where $p(n|a)=p(n)/\sum_{n \in \mathcal{N}_a} p(n)$ if $n \in \mathcal{N}_a$ and otherwise $p(n|a)=0$. The fraction of decoder messages represented by memory location n is $p(n)=1/|\mathcal{N}|$.

A. Aligned Design of Memory Location Updates

The averaging procedure can cause a performance loss as the averaged meaning $p(\bar{X}_a=x|\bar{T}_a^*=t)$ for a message t w.r.t. bit x can differ from its accurate meaning $p(X_n=x|T_n^*=t)$. A joint design aligns the characteristics of variables T_n^* within the averaging regions \mathcal{N}_a . The underlying idea is termed *message alignment* in literature [13], [23]. Hence, the averaging regions \mathcal{N}_a can also be seen as *alignment regions*. All extrinsic node input combinations are collected in the set \mathcal{Y}_n^* as defined in (3) for $\star=v$ or (6) for $\star=c$. Any input combination in the alignment region \mathcal{N}_a is given by

$$\bar{y}_a \in \bar{\mathcal{Y}}_a = \bigcup_{n \in \mathcal{N}_a} \mathcal{Y}_n^*. \quad (12)$$

The objective is to find a mapping $p(\bar{t}_a|\bar{y}_a)$ that maximizes mutual information $I(\bar{X}_a; \bar{T}_a)$ solved with an IB algorithm. The optimal mapping can be carried out with threshold quantization $\bar{t}_a=Q(L(x_a|\bar{y}_a))$. Thus, the same quantizer thresholds can be used across the alignment region. The approach minimizes the mutual information loss $I(\bar{X}_a; \bar{Y}_a) - I(\bar{X}_a; \bar{T}_a)$ introduced by representing multiple message variables T_n^* with a single variable \bar{T}_a . The design complexity is significantly

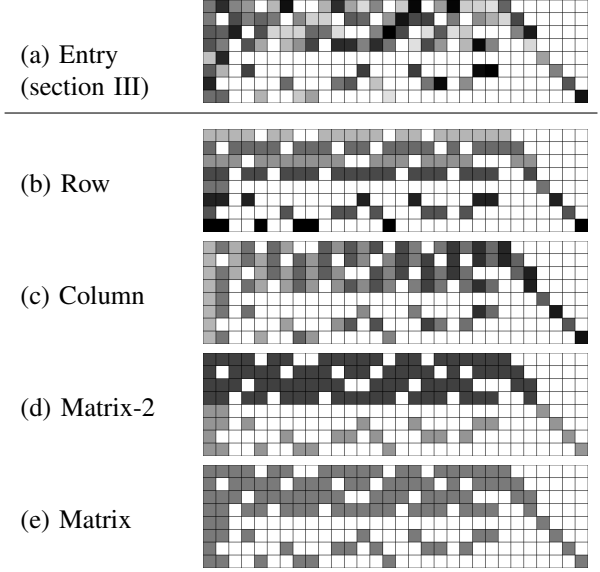


Fig. 4: Alignment regions for the random variables that represent memory locations organized in a base-matrix view.

reduced if only a single quantizer is optimized for multiple message variables T_n^* .

B. Layered Decoding

Each step of a *layered* decoding schedule updates a subset of all memory locations $\mathcal{U} \subseteq \mathcal{N}$. A quantizer design must only be performed for the regions with index $a' \in \mathcal{A}' = \{a : \mathcal{U} \cap \mathcal{N}_a \neq \emptyset\}$. Not all locations in $\mathcal{N}_{a'}$ are necessarily updated with \mathcal{U} . Thus, the quantizer designed for region $\mathcal{N}_{a'}$ is used only for updating the locations defined by \mathcal{U} .

C. Alignment Strategies

Fig. 4b to Fig. 4e illustrate several alignment strategies. VN and CN messages can use different strategies. The row alignment in Fig. 4b preserves degree-specific reliability levels for the CN messages. Low-degree CNs provide more reliable messages than high-degree CNs. Vice versa, the column-alignment in Fig. 4c preserves degree-specific reliability levels for the VN messages. High-degree VNs provide more reliable messages than low-degree VNs. On the other hand, a row alignment for the VN messages ensures the same reliability for all inputs to a CN exploited in (10). The matrix-alignment in Fig. 4e enforces the same reliability levels for all exchanged VN or CN messages, leading to the lowest complexity. The matrix-2-alignment in Fig. 4d defines two complementary regions where the first region excludes rows connected to degree-one VNs. It is a compromise between the row and matrix alignment.

D. Frame Error Rate Performance

The decoding performance of the alignment strategies (cf. Fig. 4) is compared in this section using a rate $r=1/3$ 5G-LDPC code with $K=8448$ (base graph 1), binary-phase shift-keying (BPSK) modulation and an additive white Gaussian noise (AWGN) channel.

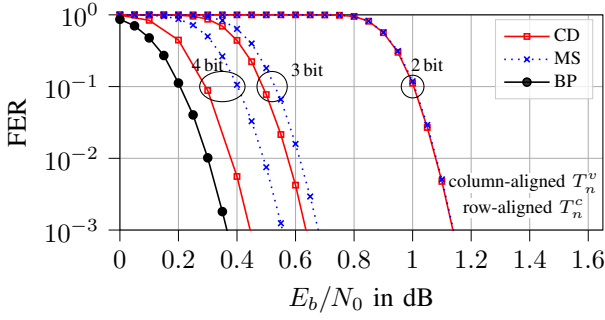


Fig. 5: Computational vs. min-sum CN update.

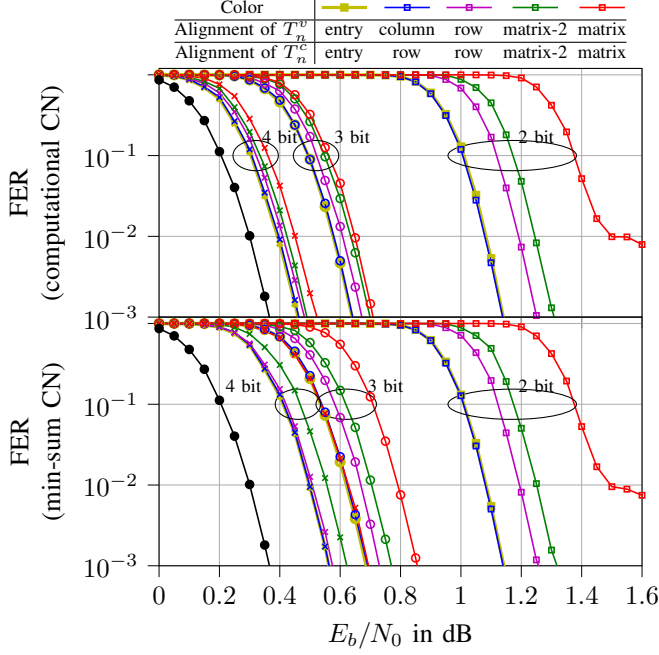


Fig. 6: Performance of different alignment strategies.

The channel messages are quantized with $w^{ch}=4$ bits. The distribution $p(t^{ch}|x^{ch})$ depends on the design- E_b/N_0 which is finely tuned to minimize frame error rate (FER). A flooding schedule performs a maximum of $\iota_{max}=30$ decoder iterations. The decoding is stopped earlier when all core parity checks are satisfied. Core parity checks correspond to CNs that involve only inputs from VNs with $d_v>1$ [31]. A frame error is counted if any of the information bits or core parity bits is falsely decoded.

The VN uses the computational domain as defined in (4). The CN uses the computational domain (7) or min-sum approximation (10), whose FER performance is compared in Fig. 5. It can be observed that the computational domain update shows increasing gains for higher message resolutions. Under 2-bit decoding, the performance is almost equivalent. Compared to a high-resolution belief propagation algorithm (BP) [1], the computational domain decoders show a performance loss of 0.07 dB, 0.27 dB and 0.77 dB for 4-bit, 3-bit, and 2-bit decoding, respectively.

The performance of the individual alignment strategies for the two update variants is shown in Fig. 6 (top: computational CN, bottom: min-sum CN).

Overall, the performance degradation from using inferior

alignments is more noticeable for lower resolutions. For example, under 2-bit decoding the column-row alignment outperforms the matrix-matrix alignment by 0.4 dB.

The entry alignment (cf. Fig. 4a) achieves the best performance but causes the highest complexity in design and implementation since every quantizer and reconstruction operation is designed individually for each memory location n .

The column-row alignment (cf. Fig. 4c & Fig. 4b) saves complexity by designing common quantizers for all memory locations in each column or row, respectively. Thus, the quantization is specifically designed for each node degree.

It can be observed in Fig. 6, that designing degree-specific quantization and reconstruction functions achieves similar performance as the entry-entry configuration.

The row-row alignment (cf. Fig. 4b) forces all inputs and outputs of a CN to be represented by the same random variable. As all quantized inputs represent the same LLR alphabet, the LLR reconstruction in the min-sum update (9) can be avoided by design. Still, in Fig. 6, superior performance of the column-row alignment over the row-row alignment can be observed. In both cases equation (10) is used in the CN where no LLR translation takes place. One explanation could be that the local optimization of the quantizer thresholds is not optimal on a global scope as confirmed in section V.

The matrix alignment (cf. Fig. 4e) yields a design with the same reconstruction functions and quantization thresholds for all memory locations in one update step. However, a significant performance degradation is observed. Particularly, the 2-bit decoding shows a relatively high error floor. The error floor can be significantly reduced by using the matrix-2 alignment (cf. Fig. 4d). This strategy comprises two complementary regions where the first region excludes rows connected to degree one VNs. In this way, CN messages within the first region are not limited by the degree-one VN reliability which improves the performance in particular under 2-bit decoding.

V. CHECK NODE AWARE DESIGN OF NON-UNIFORM QUANTIZATION AT THE VARIABLE NODE

Our work [17] showed for regular LDPC codes that the decoding performance can be improved by taking the CN behavior into account when designing the quantization at the VN. In this section, the result is generalized to be compatible with irregular LDPC codes and layered decoding.

Fig. 7 depicts a CN update using *non-quantized* messages $z_{n_k}^v$ from connected extrinsic VNs to obtain a CN message t_n^c for a target VN with bit $x_n = \bigoplus_{n' \in n} x_{n'}$. The inputs to the extrinsic VNs are denoted as y . The messages x_n, y and t_n^c form a CN aware IB setup with the corresponding relevant, observed, and compressed variables X, Y , and T . The following derives a computationally efficient solution for realizing a mapping $p(t|y)$ aiming for $\max_{p(t|y)} I(X; T)$.

As a first step, a VN update without quantization is considered. A helper variable Z_n^v models the non-quantized outputs

$$z_n^v = L(x_n | y_{col(n)}^{ch}) + \sum_{n' \in n} L(t_{n'}^c | x_n). \quad (13)$$

Next, a CN update is carried out for all CN memory locations $n \in \mathcal{N}$ using the min-sum operation (9). The CN updates take

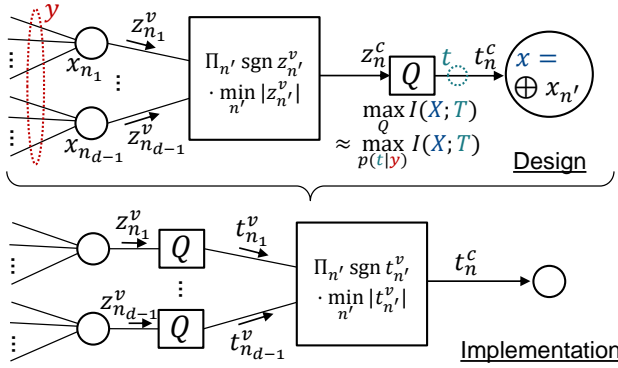


Fig. 7: Design and implementation of a CN aware IB setup.

the non-quantized VN outputs z_n^v as inputs to compute non-quantized CN messages z_n^c . Finally, a quantizer operation is designed that leads to the output messages

$$t_n^c = Q(z_n^c) = \prod_{n' \in n} \text{sgn}(z_{n'}^v) Q(\min_{n' \in n} |z_{n'}^v|). \quad (14)$$

The quantizer function $Q: \mathcal{Z}_n^c \rightarrow \mathcal{T}_n^c$ is defined by a set of symmetric quantizer thresholds τ as in section III-A. The optimization of the thresholds aims for $\max_Q I(X_n; T_n^c)$. The optimization uses the joint probability $p(x_n, z_n^c)$ which is tracked through the operations (13) and (14). As shown in Fig. 7, the resulting quantizer can be equivalently implemented before the min-sum CN update leading to drastically reduced number of exchanged bits and internal CN update complexity.

An aligned quantizer design is performed (see section IV), resulting in a specific quantizer Q for each alignment region \mathcal{N}_a of the CN memory. The specific quantizer Q is used at all the VN updates that are connected to CN updates within the alignment region. The row, matrix-2, or matrix alignment are suitable choices as all inputs to one CN use the same quantizer.

We remark, that the min-sum output z_n^c only approximates the LLR value $L(x_n|y)$ where y denotes the inputs of connected extrinsic VNs (cf. Fig. 7). Thus, threshold quantization applied on z_n^c approximates the information-optimum compression operation $p(t|y)$. Still, excellent performance improvements are achieved with this design method.

A. Analysis of Quantizer Boundary Placement

As in section IV-D a 5G-LDPC code with $K=8448$, $r=1/3$ and base graph 1 is used. A row alignment is chosen for the VN and CN memory.

Fig. 8 depicts quantizer thresholds (first row) $\tau(\iota)$ for every decoder iteration ι when using a flooding schedule. It can be observed that the CN aware design method leads to a more dense placement around the decision threshold for most of the iterations. This behavior can be explained as follows: Consider z and t as the input and output of a quantizer Q . The optimization of the quantizer aims to preserve information about a bit x by minimizing a mutual information loss

$$I(X; Z) - I(X; T) = \sum_z p(z) D_{\text{KL}}(L_z || L_t = Q(z)) \quad (15)$$

with $D_{\text{KL}}(L_z || L_t) = \sum_x p(x|L_z) \log \frac{p(x|L_z)}{p(x|L_t)}$, $L_z = L(x|z)$ and $p(x|L) = \frac{e^{-xL}}{1+e^{-xL}}$. In Fig. 9 the Kullback Leibler divergence

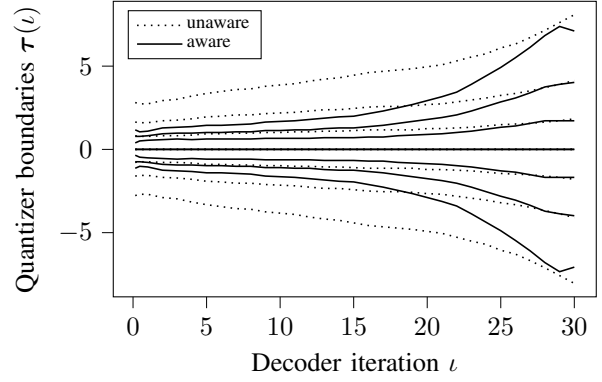
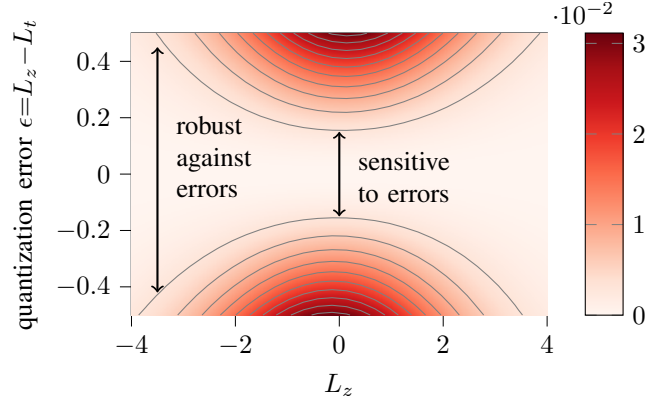


Fig. 8: Boundary placement for every iteration.

Fig. 9: Kullback Leibler divergence $D_{\text{KL}}(L_z || L_t = L_z - \epsilon)$.

D_{KL} (always non-negative) is shown in dependence of the quantization error $\epsilon = L_z - L_t$ and input LLR level L_z . The contour lines reveal that the mutual information loss is more sensitive to quantization errors when the inputs are unreliable. The fraction of unreliable messages is much larger at the CN output than at the CN input considering the min-sum update (14). Hence, the CN aware thresholds are placed more densely close to the decision threshold.

B. Frame Error Rate Performance

Fig. 10 compares the FER performance when using the CN aware and unaware design method. In the upper part of Fig. 10 a flooding schedule is used with $\iota_{\max}=30$. The performance is improved by 0.03, 0.06, and 0.2 dB when using 4, 3, or 2 bits for the exchanged messages, respectively. In the lower part of Fig. 10 a row-layered schedule is used. Although the iteration count is limited to $\iota_{\max}=15$ similar performance as with the flooding schedule with $\iota_{\max}=30$ is achieved. Also, the performance gains of the CN aware design technique are similar. From the results, it can be concluded that extending the optimization scope to include the CN outputs can improve the performance in particular for low resolutions like 2 or 3 bits without increasing the node update complexity.

VI. COMPARISON TO LITERATURE

This section compares the proposed decoder design with other approaches in the literature. These variants comprise LUT-based decoders [13], conventional min-sum decoders [5] and neural-network trained decoders [32].

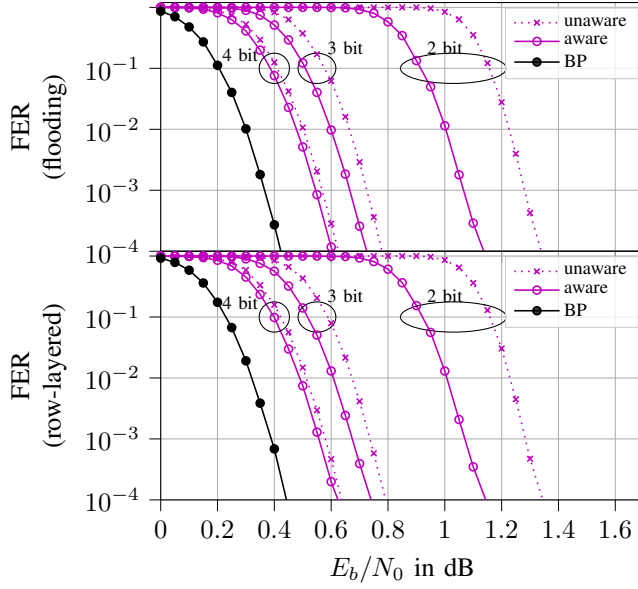


Fig. 10: Performance with CN awareness.

A. Lookup Table Based Decoders

In [13] LUT-based decoders have been proposed for 5G-like LDPC codes. All node operations are realized with concatenations of two-input LUTs. For example, a degree- d VN with underlying bit x observes the quantized extrinsic messages $y=(y_1, \dots, y_d)$ that shall be mapped to a compressed message t . As described in section III-B, a mutual information maximizing node operation performs $t=Q(L(x|y))$. Implementing this mapping with a single lookup $t=\text{LUT}(y)$ causes high complexity due to the many input combinations. Hence, [13] considers a concatenation of two-input LUTs that recursively generate the output message $t=t_d$ with $t_k=\text{LUT}_k(t_{k-1}, y_k)=Q_k(L(x|t_{k-1}, y_k))$ where $t_1=y_1$ and $k \in \{2, \dots, d\}$. The multiple compression steps Q_k cause additional mutual information loss compared to a single quantization step. This work avoids concatenated compression steps by computing $L(x|y)$ with high-resolution arithmetic operations followed by threshold quantization Q .

In [13] the performance was evaluated using a 5G-like code with $K=1032$, a code rate $r=1/3$ and a maximum iteration number $\iota_{\max}=100$. For this setup, the proposed decoders are designed using the min-sum operation at the CN with a column-row alignment (cf. Fig. 4c & Fig. 4b).

It can be observed in Fig. 11 that the proposed decoders use fewer bits for the exchanged messages to achieve similar or even better performance. For example, the proposed 4-bit decoder achieves similar performance as the 5-bit LUT decoder and outperforms the 4-bit LUT decoder by 0.39 dB. The proposed 3-bit decoder even outperforms the 4-bit LUT decoder by 0.29 dB and the 3-bit LUT decoder by 1.25 dB. The proposed 2-bit decoder shows an error floor below $\text{FER}=3 \times 10^{-4}$. However, above the error floor, it still manages to operate within 0.1 dB w.r.t. the 4-bit LUT decoder.

From the results, it can be concluded that the LUT-based decoders suffer severely from multiple intermediate quantization steps when using low code rates and when the internal resolution is below 5 bits. We remark that the decoders in

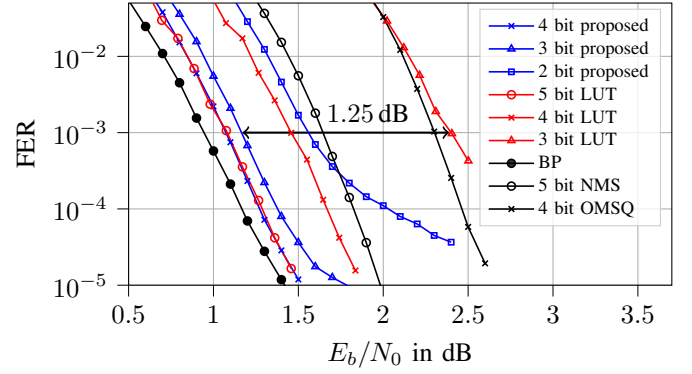


Fig. 11: Comparison to LUT and min-sum decoders [13] [5].

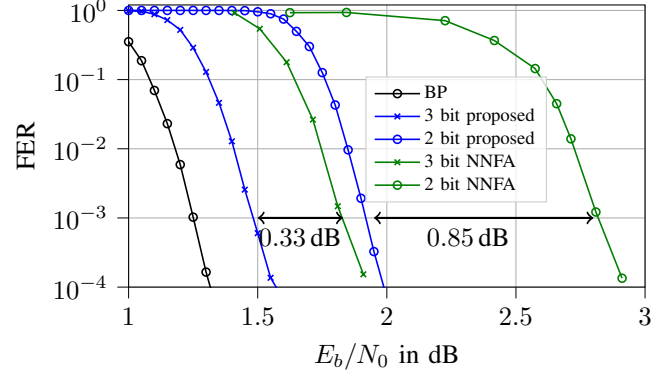


Fig. 12: Comparison to finite alphabet decoders [32].

[13] used a quantizer design that realizes a matrix alignment (cf. Fig. 4(e)). Furthermore, all proposed decoders use 4 bits for the channel message. The proposed decoders can achieve excellent performance even at resolutions as low as 2 bits under a column-row alignment.

B. Conventional Min-Sum Decoder

In [5] reduced complexity LLR-based decoding algorithms were developed which make use of approximations to simplify the design and implementation of the min-sum decoder. Two commonly used variants are known as the normalized or offset min-sum algorithm. One of the main differences compared to the proposed algorithms is that the quantization levels are not adjusted as the number of iterations increases. Hence, a higher bit width is required to offer a sufficient representation range for the exchanged LLRs. Using low resolutions like 4 bits leads to significant performance degradation which can be observed in Fig. 11. The min-sum decoders were configured as in [13]. The 4-bit quantized offset-min-sum decoder is outperformed by 1.2 dB compared to the proposed 4-bit decoder. Using a 5-bit quantized normalized-min-sum decoder reduces the difference to 0.7 dB.

C. Neural Network Trained Finite Alphabet Decoders

In [30], [33] so-called non-surjective finite-alphabet decoders were proposed. These decoders compute finite alphabet CN and VN messages as $t_n^c = \prod_{n' \in n} \text{sgn}(t_{n'}^v) \min_{n' \in n} (|t_{n'}^v|)$ and $t_n^v = Q(\phi_{ch}(t_j^{ch}) + \sum_{n' \in n} \phi(t_{n'}^c))$, respectively. The quantization $Q: \mathcal{Z} \rightarrow \mathcal{T}^v$ is classified as a non-surjective function and $\phi: \mathcal{T}^c \rightarrow \mathcal{Z}$ reconstructs the quantization levels. While the

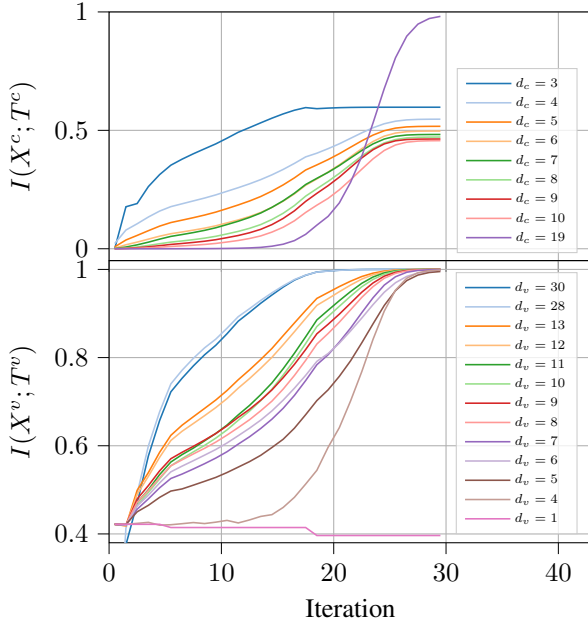


Fig. 13: Mutual information of CN and VN messages.

structure is similar to our work, the quantization Q and reconstruction ϕ are designed differently. For example [33] used heuristic techniques to optimize Q and ϕ for irregular codes. In [32] the design was improved by training Q and ϕ with a recurrent quantized neural network model for every two iterations of a flooding schedule ($\iota_{max}=20$). Fig. 12 depicts the performance of our decoders and the neural network finite alphabet (NNFA) decoders from [32] for a 5G code with rate $r=\frac{1}{2}$ and $K=8448$. The proposed decoders outperform the NNFA decoders by up to .85 dB at 2-bit resolution.

One reason for the better performance might be the usage of a probability-based design instead of a data-driven design. We optimize each Q with an IB algorithm based on probability distributions tracked with discrete density evolution. Also the reconstruction levels ϕ are accurately obtained from the tracked probabilities instead of training them. Furthermore, we design individual ϕ and Q per iteration for every row of the base matrix with a row alignment. The NNFA decoders use the same ϕ and Q for every two iterations.

VII. SCHEDULE OPTIMIZATION FOR 5G LDPC CODES UNDER QUANTIZED DECODING

The memory model introduced earlier in section III can keep track of the mutual information that is achieved after each update. Fig. 13 depicts the evolution of mutual information under a flooding schedule. It can be observed that the mutual information w.r.t. output message of CNs and VNs shows different slopes over the iterations depending on the node degree. In layered decoding, the layers typically form groups of nodes with specific degrees. Therefore, this section shall analyze the potential of optimizing the schedule to prioritize the update of layers with the highest incremental mutual information gains. The optimization is only beneficial when there is high disparity among the node degrees (high irregularity).

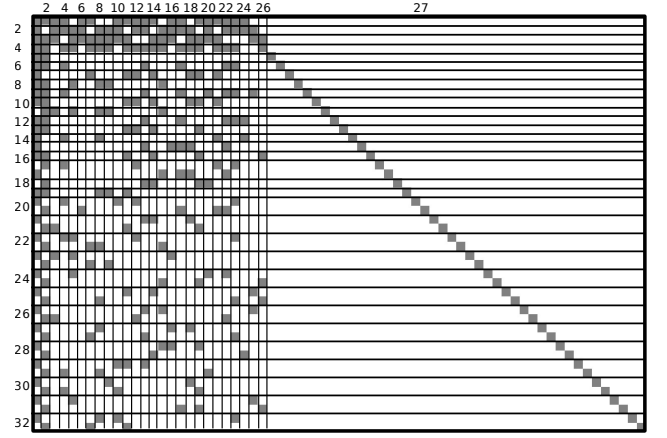


Fig. 14: Independent rows and columns form layers.

A. Row-Layered Schedule Optimization

A row-layered schedule divides a base matrix into 32 layers as enumerated in Fig. 14 for the base graph 1. Some of the consecutive rows are orthogonal and can be merged to one layer without decreasing the convergence speed [34]. A single layer update comprises VN updates \mathcal{U}^v followed by CN updates \mathcal{U}^c pointing to the memory locations \mathcal{M}_l in layer l . Typically, the updates are performed one after another (cf. Fig. 14). To accelerate the convergence, it is suggested to select the layer $l_{opt} = \arg \max_l \Delta I_l^c$ in each update step which provides the highest mutual information gain

$$\Delta I_l^c = \sum_{n \in \mathcal{M}_l} p(n) (I(X_n^c; \tilde{Z}_n^c) - I(X_n^c; Z_n^c)). \quad (16)$$

In (16) the variables Z_n^c are the non-quantized CN outputs as defined in (14) and the tilde \tilde{Z}_n^c denotes that the variable Z_n^c has been improved through the update of layer l . Using a quantized message would require temporary quantizer designs for every layer which increases design complexity and did not show performance improvements. The schedule construction finishes when reaching the maximum number of iterations.

B. Column-Layered Schedule Optimization

A column-layered schedule divides the base matrix into 27 vertical layers as enumerated in Fig. 14 for base graph 1. A single layer update comprises CN updates \mathcal{U}^c followed by VN updates \mathcal{U}^v pointing to the memory locations \mathcal{M}_l in layer l . It is proposed to select the layer $l_{opt} = \arg \max_l \Delta I_l^v$ in each layer update step which provides the highest mutual information gain

$$\Delta I_l^v = \sum_{n \in \mathcal{M}_l} p(n) (I(X_n^v; \tilde{Z}_n^v) - I(X_n^v; Z_n^v)) \quad (17)$$

where the tilde \tilde{Z}_n^v denotes that the variable Z_n^v has been improved with the update of layer l . The non-quantized VN outputs Z_n^v are defined in (13).

C. Performance of Optimized Schedules

Fig. 15 evaluates the performance when using the standard and optimized layered decoding schedules. All setups use the

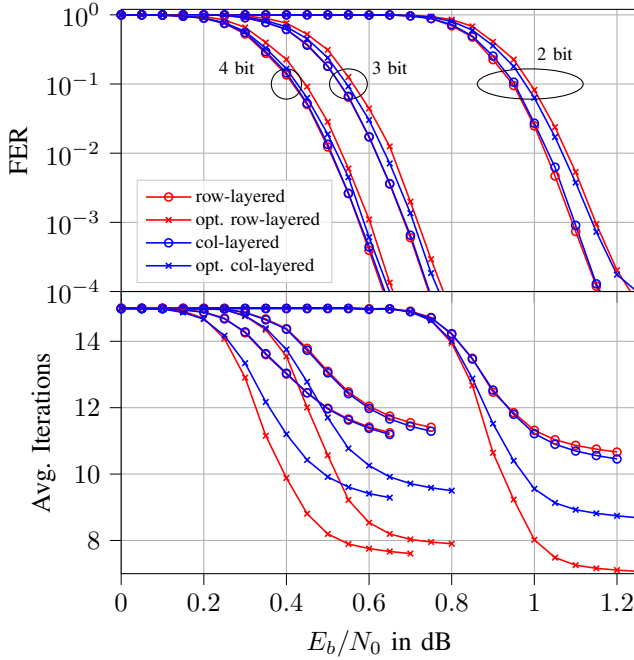


Fig. 15: Performance of optimized layered decoding schedules.

same design- E_b/N_0 and a CN aware quantizer design with row alignment.

It can be observed that the standard row- and column-layered schedules deliver similar performance in terms of FER and average iteration count.

The optimized column-layered schedule reduces the average iteration count for all bit widths by approximately 20%. The optimized row-layered schedule achieves a reduction of 35%.

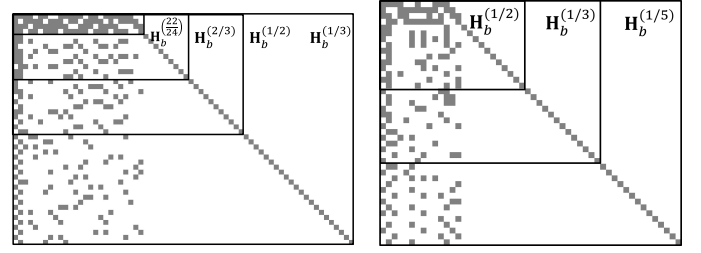
A 0.03-0.05 dB performance loss is observed compared to the standard schedule. The optimization can lead to a non-uniform number of updates of the individual layers, possibly creating more harmful cycle effects that are neglected in the probabilistic decoder model of the design phase.

VIII. RATE COMPATIBILITY

Adapting the code rate is essential in 5G for reliable and efficient transmission under varying channel conditions. 5G LDPC codes with different rates are derived from a base matrix, as shown in Fig. 16. Instead of using multiple rate-specific decoders, employing a single rate-compatible decoder reduces receiver complexity. This section presents a rate-compatible decoder for the new proposed techniques, which include alignment regions, CN aware quantization, and layered schedules. The rate-compatible design ensures consistent reconstruction and quantizer parameters for all code rates in each update of a decoding schedule \mathcal{U} .

A. Modification of the Design Process

Multiple design code rates are selected with $r \in \mathcal{R}$ either for base graph 1 or base graph 2. Each r identifies a parity check matrix $\mathbf{H}_b^{(r)}$, depicted in Fig. 16. As introduced in section II-B, the non-zero entries of each $\mathbf{H}_b^{(r)}$ can be seen as memory locations $n^{(r)} \in \mathcal{N}^{(r)}$ for the exchanged messages in a decoder.



(a) Base graph 1

(b) Base graph 2

Fig. 16: Multiple rates with base graph 1 or base graph 2.

Every code can be decoded with the lowest-rate decoder by deactivating parts of the lowest-rate matrix $\mathbf{H}_b^{(r_0)}$.

Multiple decoders are designed jointly with the previously described techniques by extending the memory location index n with a rate dimension such that $n \in \mathcal{N} = \mathcal{N}^{(r_0)} \times \mathcal{R}$. Thus, each n identifies a memory location as well as the code rate. The fraction of messages represented by location n is

$$p(n) = p(n^{(r_0)}, r) = \begin{cases} 1/\sum_r |\mathcal{N}^{(r)}| & n^{(r_0)} \in \mathcal{N}^{(r)} \\ 0 & \text{else} \end{cases}. \quad (18)$$

A rate-compatible design follows straightforwardly from the alignment approach in section IV. Any alignment region \mathcal{N}_a is extended to incorporate all code rates $\mathcal{N}_a = \mathcal{N}_a^{(r_0)} \times \mathcal{R}$ where $\mathcal{N}_a^{(r_0)}$ denotes the memory alignment w.r.t. the lowest rate matrix $\mathbf{H}_b^{(r_0)}$. The rate-extended probability $p(n)$ and alignment region \mathcal{N}_a are used in (11) and (12).

For each code rate r an individual design- E_b/N_0 must be specified, leading to individual channel distributions $p(b, L^{ch}|r)$. All code rates use the same channel quantizer. For the quantizer design, the design distribution is obtained by averaging over the individual channel distributions $p(b, L^{ch}|r)$. It was observed that each design- E_b/N_0 for the rate-compatible decoder had to be slightly higher than the design- E_b/N_0 of the corresponding rate-specific decoder.

We remark that the distributions w.r.t. dimension r are tracked independently through the node operations in the design phase. Individual tracking is required to correctly compute the average node output distributions as the node degree depends on the rate r .

B. Performance of Rate Compatible Designs

Fig. 17 evaluates the rate-compatible design for 2-bit and 3-bit decoding designed with code rates $\mathcal{R} = (\frac{1}{3}, \frac{1}{2}, \frac{2}{3}, \frac{22}{24})$ using base graph 1. The representation in terms of E_s/N_0 is intentional for better visual separability among the code rates and to highlight the channel conditions where the designed decoders can operate with incremental redundancy (IR) hybrid automatic repeat request (HARQ) techniques [26].

The rate-compatible designs are compared to rate-specific designs with standard and optimized row-layered schedules. It can be observed that the performance gap compared to the belief propagation decoder is getting smaller for higher code rates. The rate-compatible designs operate within 0.01 dB to 0.1 dB compared to the rate-specific designs. The 3-bit decoders show a lower error floor than the 2-bit decoders.

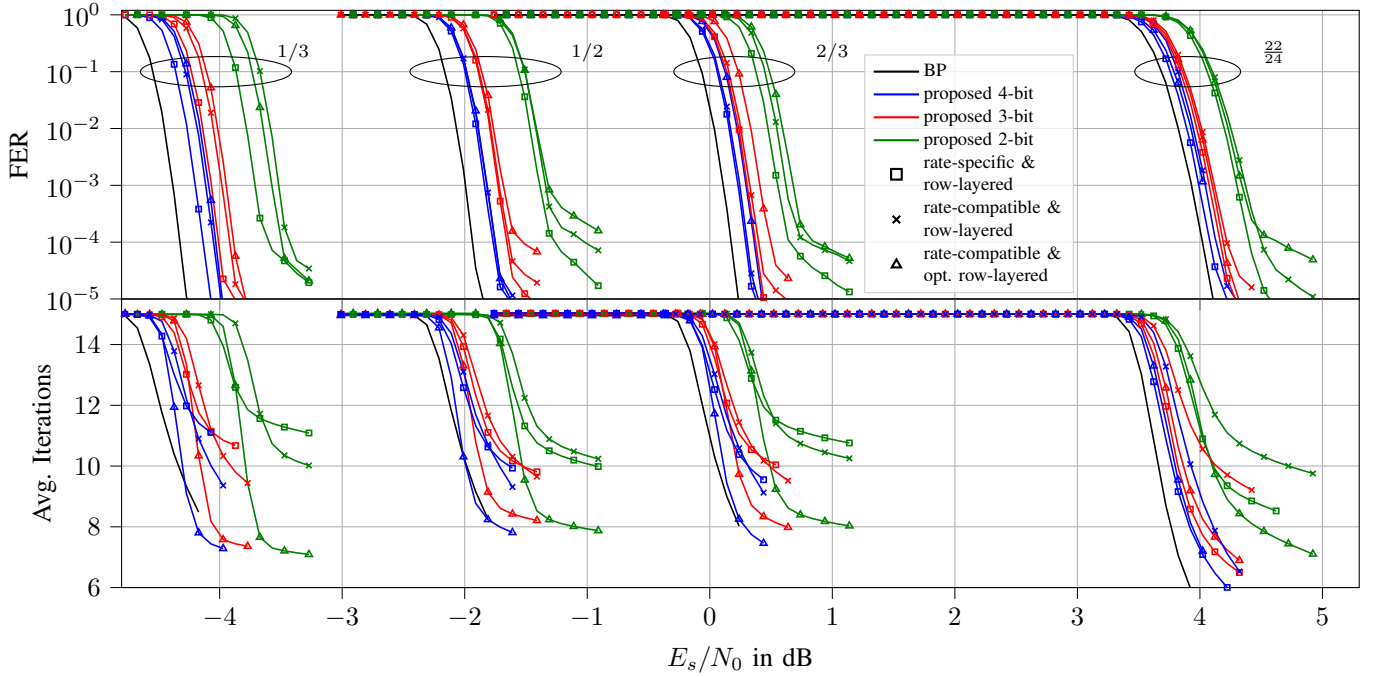


Fig. 17: Rate-compatible decoding with 2, 3, and 4 bits.

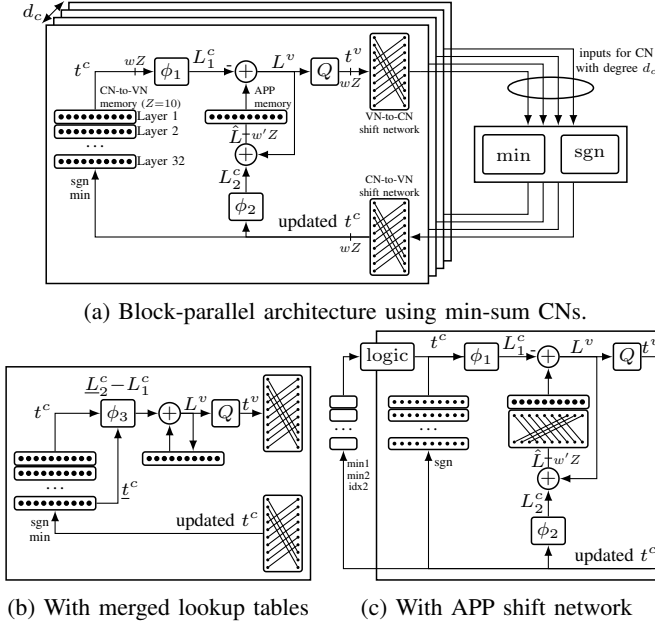


Fig. 18: Efficient structures for row-layer updates (\$Z=10\$).

The optimized layered schedule reduces the average iteration count by up to 35% for the code rate $r=\frac{1}{3}$. As mentioned earlier, the high irregularity of the lower rate codes makes the schedule optimization more effective. The error floor increases in some cases as cycle effects are neglected within the layer optimization procedure.

IX. IMPLEMENTATION COMPLEXITY

This section proposes efficient implementation options depicted in Fig. 18. A row-layered schedule is chosen as it achieved a lower iteration count under the schedule optimization in section VII. A block-parallel decoder is considered which processes Z messages for each entry of the base matrix

in parallel [35]. The block-parallel decoders balance throughput, area efficiency, and decoding flexibility when reusing a reconfigurable shift network. They are particularly suited for the maximum block lengths in 5G NR which require large shift networks with $Z=384$.

Considering Fig. 18a, the decoding is initialized by setting the channel LLR, compactly denoted by $L(t^{ch})$, as the a-posteriori-probability (APP) LLR \hat{L} . In the following, a layer update is briefly summarized. A reconstruction ϕ_1 generates the w' -bit non-extrinsic LLR L_1^c from $t^c \in \{\pm 1, \dots, \pm 2^{w'-1}\}$. The reconstruction uses a lookup table of size $(w'-1)2^{w'-1}$ bits by exploiting symmetries $|L(\alpha)| = |L(-\alpha)| = L(|\alpha|)$ where $\alpha := t^c$. Hence, with $\alpha_0 = \text{sgn}(\alpha)$,

$$\phi_1(\alpha) = L(\alpha) = \alpha_0 |L(\alpha)| = \alpha_0 L(|\alpha|). \quad (19)$$

The input L^v to the quantizer is efficiently computed by subtracting the reconstructed non-extrinsic message L_1^c from the shifted w' -bit APP LLR \hat{L} . A quantizer Q generates a compressed w -bit message $t^v = \text{sgn}(L^v)Q(|L^v|)$ through $w-1$ comparisons to a subset of the $2^{w'-1}-1$ thresholds. Finally, t^v is exchanged as one of the Z messages through a shifting network. The CN uses the min-sum approximation, where d_c inputs are processed from other connected VNs to compute (10) which can be implemented as a two-minima search [36]. An updated CN message t^c is sent back through the shifting network. The reconstruction $L_2^c = \phi_2(t^c)$ and L^v yield an updated APP message \hat{L} clipped to w' bits. Furthermore, t^c is stored in memory for the next update of layer l .

In structure Fig. 18b, the two reconstructions and the addition are replaced by a single reconstruction ϕ_3 using a table of size $w'2^{2w'-1}$. The inputs are the updated CN message $\alpha := t^c$ of the previous layer, and the non-extrinsic message $\beta := t^c$ for

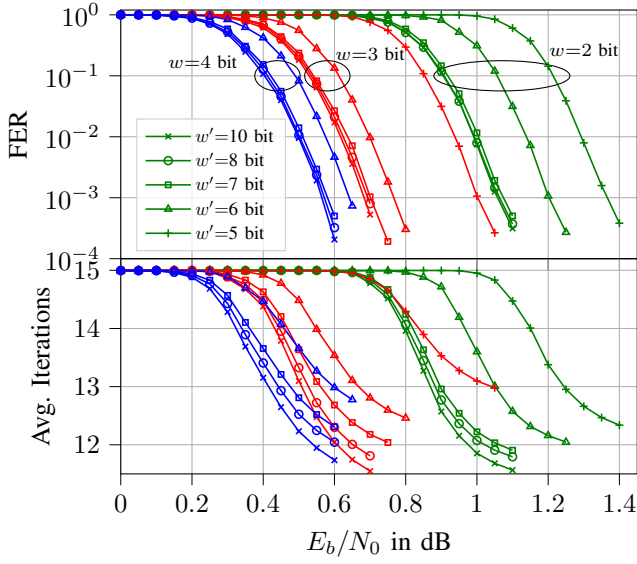


Fig. 19: Performance with different internal adder resolutions.

the current layer. Exploiting symmetries as in (19), gives

$$\begin{aligned}\phi_3(\alpha, \beta) &= L(\alpha) - L(\beta) = \alpha_0(L(|\alpha|) + \alpha_0\beta_0 L(|\beta|)) \\ &= \alpha_0 \phi'_3(|\alpha|, |\beta|, \alpha_0\beta_0).\end{aligned}\quad (20)$$

For $w=2$ the table size for ϕ_3 is similar to ϕ_1 and ϕ_2 in structure Fig. 18a under $w=3$. Hence, 2-bit decoding can save an addition operation without increasing the lookup complexity.

In structure Fig. 18c, the expensive shifting operation is performed with the APP message of size w' [37]. One main advantage is that the CN-to-VN memory is smaller as all d_c CN outputs are processed in the same shifted domain. In that approach, all outputs of a CN can be stored using d_c sign bits, the first and the second minimum as well as the index identifying the output for the second minimum. Overall, $d_c + 2(w-1) + \lceil \log_2 d_c \rceil$ bits are required. The other approaches used $d_c w$ bits for one CN. Depending on the lifting factor Z and the hardware platform, the shifting network may dominate the complexity. In that case, structure Fig. 18a and Fig. 18b save expensive interconnects if $2w < w'$, i.e. t^v and t^c are have lower resolution than \hat{L} .

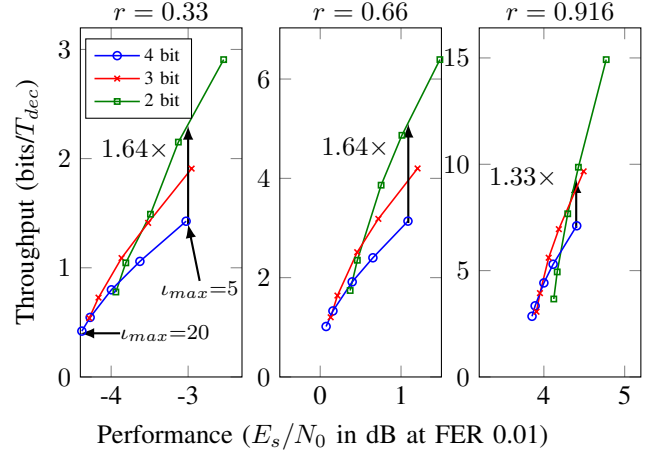
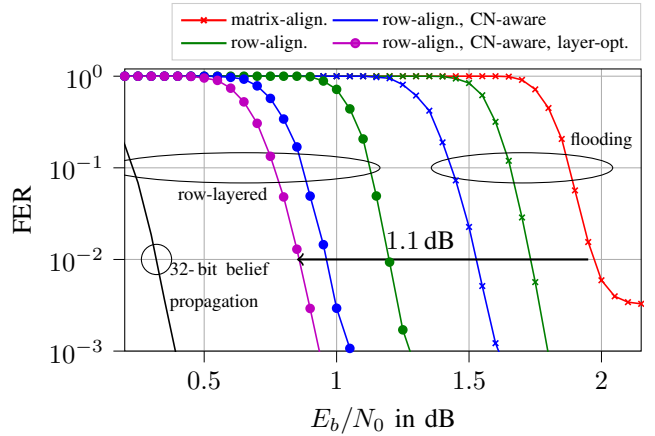
A. Internal Resolution Selection

Fig. 19 evaluates the performance for different external and internal resolutions w and w' , respectively. The reduction in resolution w' comes at the expense of an increased number of iterations. It can be observed, that among external resolutions $w=2, 3$ or 4 , $w' \leq 6$ causes significant performance degradation. Hence, for the low-resolution processing with $w=2$ or 3 bits, choosing structure Fig. 18a or Fig. 18b seems reasonable.

B. Throughput and Performance Trade-off

Fig. 20 compares the throughput and the E_s/N_0 at target FER for rate-specific decoder designs. We investigate the rates $r \in \{\frac{1}{3}, \frac{2}{3}, \frac{11}{12}\}$ using base graph 1 with $K=8448$.

The throughput is defined as K/T_{dec} where K is the number of decoded info bits. A normalized decoding latency

Fig. 20: Throughput vs. performance when changing ι_{max} .Fig. 21: Improvements for 2-bit decoding ($\iota_{max}=15$, $r = \frac{1}{3}$).

is estimated as $T_{dec} = T_{block} \iota_{avg} |\mathcal{N}^{(r)}|$ where ι_{avg} is the average iteration count at a target FER=0.01 and $|\mathcal{N}^{(r)}|$ is the number of block updates per iteration. We assume the block-processing delay as $T_{block}=w$ for several reasons. The forward and backward shifts of the w -bit messages are performed in serial via a single bit-wise shifting network to establish a similar routing area among the compared bit widths w . The quantization involves $w-1$ comparisons in serial [16]. The min-sum update is dominated by a sequence of w -bit comparisons. The reconstruction delay depends on w as well.

The area efficiency, i.e., the ratio of throughput and chip area can further improve with lower bit width. However, estimating the chip area is beyond the scope.

To obtain the throughput-performance curves in Fig. 20, the decoding delay is finely controlled by setting the maximum number of iterations to $\iota_{max} \in \{20, 15, 10, 7.5, 5\}$. It can be observed that the resolution w that achieves the highest throughput depends on the operation- E_s/N_0 . For low operation- E_s/N_0 , 4-bit decoding achieves the highest throughput as 3-bit or 2-bit yield diminishing returns when increasing the maximum iteration count ι_{max} .

However, hardware implementations as in [35] typically limit $\iota_{max} \approx 5$ to minimize decoding delay and maximize energy efficiency. In that regime, 2-bit decoding offers a very promising trajectory showing up to 64% higher throughput than 4-bit decoding at similar FER performance.

X. CONCLUSIONS

This paper revealed significant improvement potential for low-resolution decoding of 5G-LDPC codes by three main contributions. First, a probabilistic base matrix memory model enabled a region-specific optimization of the reliability levels represented with low-resolution messages. Using distinct regions allows low-resolution messages to cope with the high irregularity of 5G-LDPC codes. Secondly, a check node aware design of quantizer thresholds at the variable nodes further enhanced the performance. Third, the order of layers in the decoding schedule is optimized for row and column-layered schedules prioritizing layer updates with high mutual information gain which increased the throughput by up to 35%. Fig. 21 depicts the overall improvements under 2-bit decoding with considerable performance gains of up to 1 dB through the combined application of the aforementioned techniques. A straightforward design of a rate-compatible decoder is demonstrated by extending the introduced concept of alignment regions. A complexity analysis showed, that the 2-bit resolution may improve the decoding throughput by 64 % compared to the 4-bit resolution at similar frame error rate performance and hardware complexity.

REFERENCES

- [1] R. Gallager, "Low-Density Parity-Check Codes," *IRE Transactions on Information Theory*, vol. 8, no. 1, pp. 21–28, 1962.
- [2] D. J. MacKay and R. M. Neal, "Near Shannon Limit Performance of Low Density Parity Check Codes," *Electronics letters*, vol. 33, no. 6, pp. 457–458, 1997.
- [3] 3GPP, "5G NR: Multiplexing and Channel Coding, TS 38.212," 2018.
- [4] J. Chen and M. Fossorier, "Density evolution for two improved BP-Based decoding algorithms of LDPC codes," *IEEE Communications Letters*, vol. 6, no. 5, pp. 208–210, 2002.
- [5] J. Chen, A. Dholakia, E. Eleftheriou, M. Fossorier, and X.-Y. Hu, "Reduced-complexity decoding of LDPC codes," *IEEE Transactions on Communications*, vol. 53, no. 8, pp. 1288–1299, 2005.
- [6] J. Thorpe, "Low-complexity approximations to belief propagation for LDPC codes," in *Proceedings of IEEE ISIT*, 2003.
- [7] J.-S. Lee and J. Thorpe, "Memory-efficient decoding of LDPC codes," in *Proceedings. International Symposium on Information Theory, 2005. ISIT 2005.*, 2005, pp. 459–463.
- [8] B. M. Kurkoski, K. Yamaguchi, and K. Kobayashi, "Noise Thresholds for Discrete LDPC Decoding Mappings," in *IEEE GLOBECOM 2008 - 2008 IEEE Global Telecommunications Conference*, 2008, pp. 1–5.
- [9] B. M. Kurkoski and H. Yagi, "Quantization of Binary-Input Discrete Memoryless Channels," *IEEE Transactions on Information Theory*, vol. 60, no. 8, pp. 4544–4552, 2014.
- [10] F. J. C. Romero and B. M. Kurkoski, "LDPC Decoding Mappings That Maximize Mutual Information," *IEEE Journal on Selected Areas in Communications*, vol. 34, no. 9, pp. 2391–2401, 2016.
- [11] J. Lewandowsky and G. Bauch, "Information-Optimum LDPC Decoders Based on the Information Bottleneck Method," *IEEE Access*, vol. 6, pp. 4054–4071, 2018.
- [12] M. Meidlinger, G. Matz, and A. Burg, "Design and Decoding of Irregular LDPC Codes Based on Discrete Message Passing," *IEEE Transactions on Communications*, vol. 68, no. 3, pp. 1329–1343, 2020.
- [13] M. Stark, L. Wang, G. Bauch, and R. D. Wesel, "Decoding Rate-Compatible 5G-LDPC Codes With Coarse Quantization Using the Information Bottleneck Method," *IEEE Open Journal of the Communications Society*, vol. 1, pp. 646–660, 2020.
- [14] X. He, K. Cai, and Z. Mei, "On Mutual Information-Maximizing Quantized Belief Propagation Decoding of LDPC Codes," in *2019 IEEE Global Communications Conference (GLOBECOM)*, 2019, pp. 1–6.
- [15] P. Mohr, G. Bauch, F. Yu, and M. Li, "Coarsely Quantized Layered Decoding Using the Information Bottleneck Method," in *ICC 2021 - IEEE International Conference on Communications*, 2021, pp. 1–6.
- [16] P. Mohr and G. Bauch, "Uniform vs. Non-Uniform Coarse Quantization in Mutual Information Maximizing LDPC Decoding," in *GLOBECOM 2022 - 2022 IEEE Global Comm. Conference*, 2022, pp. 3496–3501.
- [17] —, "A Variable Node Design with Check Node Aware Quantization Leveraging 2-Bit LDPC Decoding," in *GLOBECOM 2022 - 2022 IEEE Global Communications Conference*, 2022, pp. 3484–3489.
- [18] —, "Low-Resolution Horizontal and Vertical Layered Mutual Information Maximizing LDPC Decoding," in *2022 56th Asilomar Conference on Signals, Systems, and Computers*, 2022, pp. 163–167.
- [19] T. Monsees, O. Griebel, M. Herrmann, D. Wübben, A. Dekorsy, and N. Wehn, "Minimum-integer computation finite alphabet message passing decoder: From theory to decoder implementations towards 1 tb/s," *Entropy*, vol. 24, no. 10, 2022.
- [20] P. Kang, K. Cai, X. He, S. Li, and J. Yuan, "Generalized Mutual Information-Maximizing Quantized Decoding of LDPC Codes With Layered Scheduling," *IEEE Transactions on Vehicular Technology*, vol. 71, no. 7, pp. 7258–7273, 2022.
- [21] L. Wang, C. Terrill, M. Stark, Z. Li, S. Chen, C. Hulse, C. Kuo, R. D. Wesel, G. Bauch, and R. Pitchumani, "Reconstruction-Computation-Quantization (RCQ): A Paradigm for Low Bit Width LDPC Decoding," *IEEE Trans. on Communications*, vol. 70, no. 4, pp. 2213–2226, 2022.
- [22] N. Tishby, F. C. Pereira, and W. Bialek, "The information bottleneck method," 2000.
- [23] J. Lewandowsky, M. Stark, and G. Bauch, "Message alignment for discrete LDPC decoders with quadrature amplitude modulation," in *2017 IEEE Int. Symposium on Inf. Theory (ISIT)*, 2017, pp. 2925–2929.
- [24] D. Hocevar, "A reduced complexity decoder architecture via layered decoding of LDPC codes," in *IEEE Workshop on Signal Processing Systems, 2004. SIPS 2004.*, 2004, pp. 107–112.
- [25] C. Lv, X. He, P. Kang, K. Cai, J. Xing, and X. Tang, "Mutual Information-Maximizing Quantized Layered Min-Sum Decoding of QC-LDPC Codes," in *GLOBECOM 2022 - 2022 IEEE Global Communications Conference*, 2022, pp. 3490–3495.
- [26] E. Dahlman, *5G/5G-advanced: The New Generation Wireless Access Technology*. Academic Press Inc, 2023.
- [27] T. T. B. Nguyen, T. Nguyen Tan, and H. Lee, "Efficient QC-LDPC Encoder for 5G New Radio," *Electronics*, vol. 8, no. 6, p. 668, Jun. 2019.
- [28] J. Ha, D. Klinc, J. Kwon, and S. W. McLaughlin, "Layered BP Decoding for Rate-Compatible Punctured LDPC Codes," *IEEE Communications Letters*, vol. 11, no. 5, pp. 440–442, 2007.
- [29] B. M. Kurkoski and H. Yagi, "Quantization of Binary-Input Discrete Memoryless Channels," *IEEE Transactions on Information Theory*, vol. 60, no. 8, pp. 4544–4552, Aug. 2014, conference Name: IEEE Transactions on Information Theory.
- [30] S. K. Planjery, D. Declercq, L. Danjean, and B. Vasic, "Finite Alphabet Iterative Decoders—Part I: Decoding Beyond Belief Propagation on the Binary Symmetric Channel," *IEEE Transactions on Communications*, vol. 61, no. 10, pp. 4033–4045, 2013.
- [31] J. Frenzel, S. Mueller-Weinfurter, J. B. Huber, and R. R. Mueller, "Static Layered Schedules and Core-Only Parity Check for the 5G New Radio LDPC Codes," in *SCC 2019; 12th International ITG Conference on Systems, Communications and Coding*, 2019, pp. 1–5.
- [32] Y. Lyu, M. Jiang, Y. Zhang, C. Zhao, N. Hu, and X. Xu, "Optimized Non-Surjective FAIDs for 5G LDPC Codes With Learnable Quantization," *IEEE Communications Letters*, vol. 28, no. 2, pp. 253–257, 2024.
- [33] T. T. Nguyen-Ly, V. Savin, K. Le, D. Declercq, F. Ghaffari, and O. Boncalo, "Analysis and Design of Cost-Effective, High-Throughput LDPC Decoders," *IEEE Transactions on Very Large Scale Integration (VLSI) Systems*, vol. 26, no. 3, pp. 508–521, 2018.
- [34] H. Cui, F. Ghaffari, K. Le, D. Declercq, J. Lin, and Z. Wang, "Design of High-Performance and Area-Efficient Decoder for 5G LDPC Codes," *IEEE Transactions on Circuits and Systems I: Regular Papers*, vol. 68, no. 2, pp. 879–891, Feb. 2021.
- [35] Y. Ren, H. Harb, Y. Shen, A. Balatsoukas-Stimming, and A. Burg, "A Generalized Adjusted Min-Sum Decoder for 5G LDPC Codes: Algorithm and Implementation," 2024.
- [36] Y. Lee, B. Kim, J. Jung, and I.-C. Park, "Low-Complexity Tree Architecture for Finding the First Two Minima," *IEEE Transactions on Circuits and Systems II: Express Briefs*, vol. 62, no. 1, pp. 61–64, 2015.
- [37] S. Kim, G. E. Sobelman, and H. Lee, "A Reduced-Complexity Architecture for LDPC Layered Decoding Schemes," *IEEE Trans. on Very Large Scale Integr. (VLSI) Systems*, vol. 19, no. 6, pp. 1099–1103, 2011.